Journal of Polymer Research (2018) 25: 130
https://doi.org/10.1007/s10965-018-1518-2

ORIGINAL PAPER

Excellent corrosion protection performance of epoxy composite coatings filled with silane functionalized silicon nitride

Yongxing Zhang[1] · Min Zhao[2] · Jiaoxia Zhang[2] · Qian Shao[3] · Jianfeng Li[3] · Hang Li[1] · Bo Lin[1] · Meiyan Yu[1] · Shougang Chen[1] · Zhanhu Guo[2]

Received: 7 November 2017 / Accepted: 11 April 2018 / Published online: 1 May 2018

Abstract

Silicon nitride was firstly used as anticorrosive pigment in organic coatings. An effective strategy by combining inorganic fillers and organosilanes was used to enhance the dispersibility of silicon nitride in epoxy resin. The formed nanocomposites were applied to protect Q235 carbon steel from corrosion. The anticorrosive performance of modified silicon nitride with silane (KH-570) was investigated by electrochemical impedance spectroscopy (EIS), water absorption and pull-off adhesion methods. With the increase of immersion time, the corrosion resistance as well as adhesion strength of epoxy resin coating and unmodified silicon nitride coating decreased significantly. However, for the modified silicon nitride coating, the corrosion resistance and adhesion strength still maintained 5.7×10^{10} Ω cm^2 and 7.6 MPa after 2400-h and 1200-h immersion, respectively. The excellent corrosion resistance performance could be attributed to the chemical interactions between KH-570 functional groups and silicon nitride powders, which mainly came from the easy formation of Si-O-Si bonds. Furthermore, the modified silicon nitride coating formed a strong barrier to corrosive electrolyte due to the hydrophobic of modified silicon nitride powder and increased bonds.

Keywords Silicon nitride · Silane · Surface modification · Coating;strong barrier · Corrosion protection

Introduction

Epoxy coatings have been widely used for protecting metal structures from environmental and corrosion attacks due to their outstanding toughness, adhesion to metal substrates, and durability [1–4]. However, the epoxy coatings are prone to penetration by water and electrolyte species, and may experience degradation during long-term service [5, 6]. Therefore, fillers-incorporated epoxy coatings have been developed to enhance the anticorrosion performance of metals [7–11]. For example, iron oxides were added in the coating to decrease the defects existing at the interface between epoxy and metal substrate by high temperature milling methods [12, 13]. Epoxy coatings containing TiO_2 nanoparticles were employed to improve the anticorrosion performance and mechanical properties of the coatings [14–16]. The addition of conductive polymers such as polyaniline (PANI) was found to improve the corrosion resistance of epoxy coatings [17–19]. The adhesion of the epoxy coatings was enhanced by cerium addition [20].

Although the addition of fillers is helpful for an enhanced corrosion resistance of the coatings, inorganic fillers usually possess a poor dispersion in the coating matrix, resulting in interfacial defects and micro-voids [12–15, 21]. As a comparison, silane agents were found to improve the adhesion strength of coatings, reduce water uptake and enhance corrosion resistance of the coatings, which were associated with the hydrophobic property of the silane [22–24]. For example, epoxy coating modified with a 3-glycidoxypropyltrimethoxysilane (GPTMS) could reduce the water adsorption remarkably

Electronic supplementary material The online version of this article (https://doi.org/10.1007/s10965-018-1518-2) contains supplementary material, which is available to authorized users.

✉ Shougang Chen
sgchen@ouc.edu.cn

✉ Zhanhu Guo
zguo10@utk.edu

[1] College of Materials Science and Engineering, Ocean University of China, Qingdao 266100, China

[2] Integrated Composites Laboratory (ICL), Department of Chemical & Biomolecular Engineering, University of Tennessee, Knoxville, TN 37934, USA

[3] College of Chemical and Environmental Engineering, Shandong University of Science and Technology, Qingdao 266590, People's Republic of China

[22]. The adhesion property, anticorrosion performance and the protection mechanism of silane-modified epoxy coatings have been investigated [25, 26]. It was found that epoxy coatings doped with a single silane possessed a limited corrosion resistance. Moreover, the processing of coatings often includes many steps or involves complicated techniques. As a result, it is desirable to develop a strategy by combining inorganic fillers and organosilanes in a coating, enabling a significant enhancement of the adhesion strength and corrosion resistance. To date, there has been very limited study of the composite coatings containing organosilanes and inorganic fillers for the purpose.

Silicon nitride (Si_3N_4) is one of the most promising candidate materials for engineering applications [27–32]. Extensive studies have been performed to investigate the anti-oxidation and anticorrosion behavior of silicon nitride ceramics in a variety of environment [33–37]. Moreover, silicon nitride can be used as a ceramic-based coating on metals, improving the performance stability in comparison to a bulk ceramic or metal [38–40]. However, limited work has been focused on silicon nitride as an anti-corrosive pigment in organic coatings.

In this work, silicon nitride was firstly used as anticorrosive pigment in organic coatings. Epoxy composite coatings doped with silicon nitrides and 3-(trimethoxysilyl) propyl methacrylate silane were prepared to enhance the dispersibility of silicon nitride in epoxy resin, and the corrosion resistance of the composites coated on Q235 carbon steel was investigated in 3.5 wt% NaCl solution. Various analytical techniques, including Fourier transform infrared spectrum (FT-TR), transmission electron microscopy (TEM), thermogravimetric analysis, X-ray photo-electron spectrum (XPS), and water contact angle measurements were used to characterize the modified silicon nitride powders. Scanning electron microscopy (SEM) was conducted on the composite coatings. Electrochemical impedance spectroscopy (EIS), water absorption, and pull-off adhesion strength were used to measure the corrosion resistance and adhesion property of the coated steel.

Experiment

Materials

Commercially available silicon nitride particles with an average size of 5 μm were used in this work. From Fig. S1, it can be seen that the crystal structure of the silicon nitirde particles used in this experiment is β-Si_3N_4. The epoxy resin (Epon 6101, with an epoxy equivalent of 0.44 mol/100 g), curing agent, and polyamide (PA) were purchased from Phoenix Resins Inc. (Wu Xi, China). The weight ratio of PA to epoxy resin was 1:2. The solvent was a mixture of dimethylbezene and n-butyl alcohol with a weight ratio of 7:3. Q235 carbon steel, with a chemical composition (wt%) of ≤0.18% C, ≤1.4% Mn, ≤0.35% Si, ≤0.050% S, and ≤0.045% P, was used to make steel specimens. Ethyl alcohol (C_2H_5OH), acetic acid, and methacryloxy propyl trimethoxyl silane (Silane coupling agent, KH-570, $CH_2=C(CH_3)COO(CH_2)_3Si(OCH_3)_3$) were purchased from Sinopharm Chemical Reagent Co. Ltd.

Modification of silicon nitride with KH-570

Figure 1 shows the schematic diagram for the preparation of modified silicon nitride with KH-570. A certain amount of silicon nitride powders were maintained in a vacuum chamber at 80 °C for 24 h in order to eliminate the adverse interfacial effect between inorganic and organic matters. The preparation followed the procedure shown as follows. Firstly, 10 g silicon nitride powders were dispersed in 10 g KH-570, with an ultrasonic vibration for 20 min. Secondly, 3.5 g deionized water was added in 50 g ethyl alcohol (C2H5OH). Acetic acid was then added to adjust the pH value to a range between 3.5 and 5.0. The mixture was added into a three necked flask at 80 °C maintained with a water bath, and stirred at 1000 rpm for 3 h. Thirdly, the obtained hybrid solution was subjected to centrifugation to get the modified silicon nitride solution, followed by washing with deionized water repeatedly in order to remove unreacted KH-570. Finally, the modified silicon nitride powders were dried in an oven at 60 °C for 10 h.

Characterization of the modified silicon nitride powders

The FT-IR was measured on the KH-570 modified silicon nitride powders using a Nicolet 170SX instrument (Madison, WI, USA) on IR 200 spectrometer in KBr medium at ambient temperature in the region of 4000–500 cm^{-1}. The chemical composition of the modified silicon nitride powders were determined by XPS (PHI-5702 multifunctional spectrometer) using Al Ka radiation. Thermogravimetric analysis (TGA) was performed using a CHNS/O analyzer (Dupont 2200) under an air atmosphere, while the samples were heated from 30 to 800 °C at a rate of 10 °C/min. The surface morphology of the modified silicon nitride powders was characterized with TEM (HITACHIH-7650). An optical contact angle instrument (OCA40, DataPhysics GmbH) was also used to measure the water contact angle of modified silicon nitride powders to measure the hydrophobicity.

Preparation of epoxy-based composite coatings

Epoxy composite coatings doped with either as-received silicon nitrides or KH-570 modified silicon nitrides by 5 wt% were prepared by ball milling at ambient temperature. Agate grinding medium with balls to the mixture ratio of 5:1 was used in this grinding test work. The grinding rotational speed was 360 rpm/min and the grinding time was 6 h. After

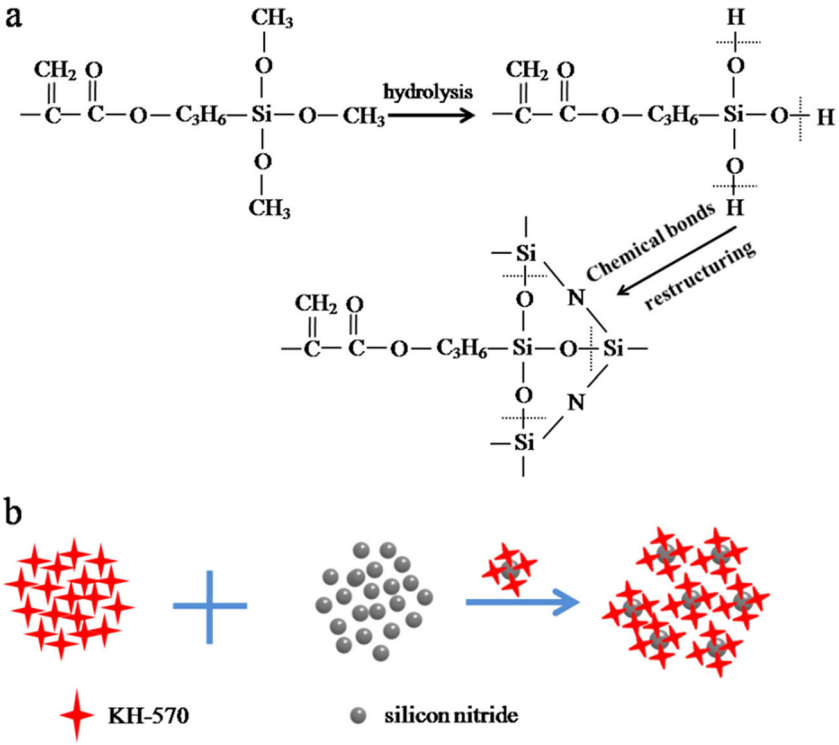

Fig. 1 Schematic diagram of the preparation of modified silicon nitride powders with KH-570

grinding, the pre-determined amount of curing agent PA and solvent (i.e., the mixture of dimethylbezene and n-butyl alcohol) were added. After applying on Q235 steel panels, the coatings were cured at 30 °C for 1 day, and then cured at 60 °C for 1 day. The thickness of the dry coating was within the range of 120 ± 10 μm. The prepared coatings were also applied on a silicon rubber board. After drying, the coatings were peeled off from the board, and an area of 2 cm×2 cm was created to measure water absorption of the coatings.

Characterization of corrosion resistance and other properties of the coatings

Electrochemical measurements were performed on a conventional three-electrode cell using a GAMRY RFE 2000 system at ambient temperature in 3.5 wt% NaCl solution for various days to evaluate the corrosion resistance of the coatings. The coated steel was used as working electrode, a platinum plate (2 cm×2 cm) was used as counter electrode, and an Ag/AgCl (saturated KCl) electrode was used as reference electrode.

After the coated steel electrode achieved a steady open circuit potential, EIS measurements were performed over a frequency range of 100 kHz to 10 mHz under a 20 mV amplitude sinusoidal voltage disturbance. The experimental data were analyzed using the commercial software @ZsimpWin [12, 41–43] .

Water absorption of the coatings was measured by determining the weight change of the coatings as a function of immersion time in 3.5 wt% NaCl solution at ambient temperature. The initial weight before and after immersion testing was accurately measured by an electronic balance, with an accuracy of 10^{-4} g.

The coating adhesion to the steel substrate was determined by a PosiTest Pull-Off Adhesion Tester (DeFelsko Corporation, USA). The adhesion measurements were examined at ambient temperature by immersing the coated steel in 3.5 wt% NaCl solution for 0, 200, 500, 700 and 1200 h, respectively. The specimen size of pull-off test adhesion test was 5 cm×5 cm×0.2 cm. Six parallel coated steel panels were used

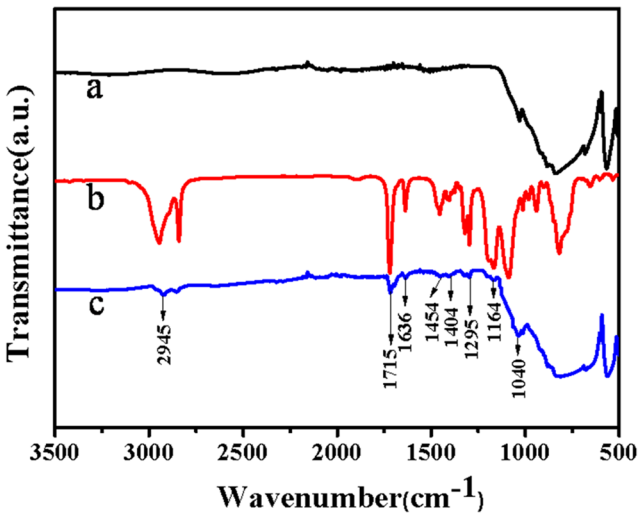

Fig. 2 FT-IR spectra of silicon nitride modified with KH-570 (a: silicon nitride, b: KH-570, c: modified with KH-570)

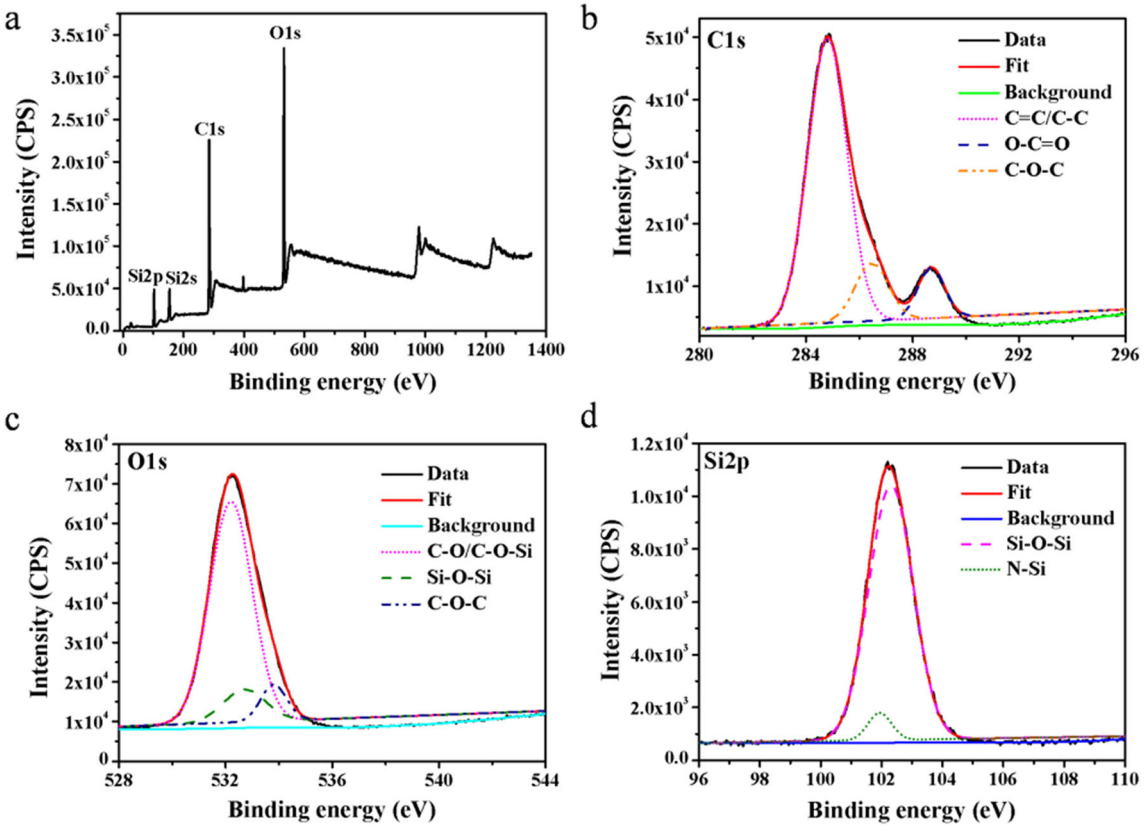

Fig. 3 XPS spectra of modified silicon nitride: (**a**) Full scan; (**b**) C 1 s; (**c**) O 1 s; (**d**) Si 2p

under each condition by calculating the average of adhesion strength to ensure the data reproducibility [19, 44–46].

Results and discussion

Characterization of KH-570 silane modified silicon nitride powders

Figure 2 shows the FT-IR spectra of silicon nitride, KH-570 and the KH-570 modified silicon nitride. The characteristic silicon nitride absorption bands appear at 1060–563 cm^{-1} (i.e., –SiN stretching) [47, 48]. The absorption peak at 2945 cm^{-1} is attributed to CH_3. The characteristic KH-570 absorption bands observed at 1715 and 1636 cm^{-1} correspond to the C=O stretching vibration and C=C stretching vibration, respectively [49, 50]. The weak peaks at 1454 and 1404 cm^{-1} are assigned to C-H (CH_3) in-of-plane bending vibration and C-H bending vibration absorption, respectively. The peak absorption at 1250 and 1295 cm^{-1} are C-O stretching vibration. The bands at 1164 cm^{-1} is due to Si–O–Si absorption, which indicates a condensation reaction between silanol groups [50]. The absorption peaks of KH-570 as mentioned above are also observed in the spectrum of the KH-570 modified silicon nitride. In addition, strong chemical interactions of KH-570 functional groups and silicon nitride powders, which mainly

Table 1 Results obtained from deconvolution of XPS spectra for modified silicon nitride

Name of convoluted spectrum	Characterized bonds	Binding energy (eV)	% composition in each element
C 1 s	C=C/C-C	284.8	77.1
	O-C=O	288.7	13.5
	C-O-C	286.4	9.4
O 1 s	C-O/C-O-Si	532.2	80.2
	Si-O-Si	532.7	12.0
	C-O-C	533.8	7.8
Si 2p	Si-O-Si	102.3	91.0
	Si-N	101.9	9.0

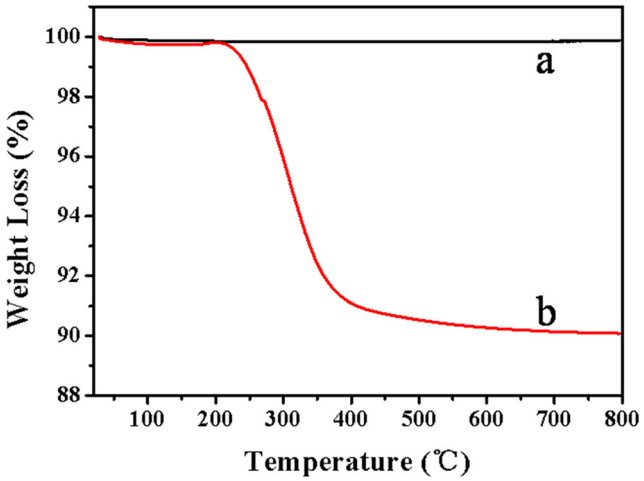

Fig. 4 TGA curves of (**a**) unmodified and (**b**) KH-570 modified silicon nitride powders

come from the easy formation Si-O-Si bonds at about 1040 cm^{-1} [51, 52]. Therefore, the as-received silicon nitride powders are modified by KH-570 through the surface wrapping of silicon nitride powders with KH-570 silane.

Figure 3 shows the XPS spectra of modified silicon nitride, and the results of deconvoluted spectra are listed in Table 1. The C1s spectra of the modified silicon nitride include various components, Fig. 3b, which are assigned to C=C/C-C (284.8 eV), O-C=O (288.7 eV) and C-O-C (286.4 eV), respectively [44, 53–55]. Figure 3 c shows the O 1 s spectra. The three peaks centered at 532.2, 532.7 and 533.8 eV are associated with C-O/C-O-Si, Si-O-Si and C-O-C, respectively. Moreover, the Si 2p spectra are separated into Si-N (101.9 eV) and Si-O-Si (102.3 eV) in Fig. 3d [57, 58]. The XPS analysis results also indicate that silicon nitride is modified with KH-570, which is consistent with the FT-IR analysis.

Figure 4 shows the TGA curves of unmodified and modified silicon nitride powders. It is seen that a nearly 9.92% weight loss occurs at 410 °C, while the weight of unmodified silicon nitride changes little, which is attributed to the decomposition of KH-570 chains. Figure 5 shows the TEM images of unmodified and modified silicon nitride powders. It could be seen that the KH-570 silane coupling agent successfully deposited on the surface of silicon nitride particles. It is expected that a coated microstructure has been formed gradually as the silane is applied on the surface of silicon nitride powders. An obvious interface could be observed. We deduced that the core-shell microstructure might appear gradually as the silane shifted to Si_3N_4 surface compared with unmodified silicon nitride powder (Fig. 5(a)). The result is also consistent with the analysis of FT-IR, XPS and TG, which further confirmed the successful modification of silicon nitride with KH-570.

In order to investigate the hydrophobic performance of the silane modified silicon nitride powders, the water contact angle was measured. Figure 6 shows the water contact angles of the as-received and the silane modified silicon nitride, respectively. It is seen that the water contact angles of the as-received and modified silicon nitride are 14° and 112°, respectively. Obviously, the silane modification significantly increases the hydrophobicity of the silicon nitride powders. This is attributed to the effect of steric obstruction and limited number of OH groups on the surface of silicon nitride [50]. Generally, more hydrophobic surfaces possess high contact angles in the range of 90-120°, which result in low surface energy and wettability [49]. The results confirm that the interaction of silicon nitride with KH-570 occurs, generating a hydrophobic surface with a low surface energy [50], which mainly comes from the easy formation Si-O-Si bonds of silicon nitride powders and KH-570 functional groups.

The dispersibility of the modified silicon nitride in epoxy matrix

Figure 7 (a-c) shows the SEM images of the cross-sections of epoxy coating, unmodified silicon nitride coating, and modified silicon nitride coating, respectively. It is seen in Fig. 7(b) that the as-received silicon nitride agglomerates in epoxy, which results in cracking between fillers and the epoxy. However, the modified silicon nitride is dispersed uniformly in the epoxy matrix, as seen in Fig. 7(c). The EDS results of coatings are shown in FigS2 and FigS3 to prove the existence of fillers from the Si and N element.

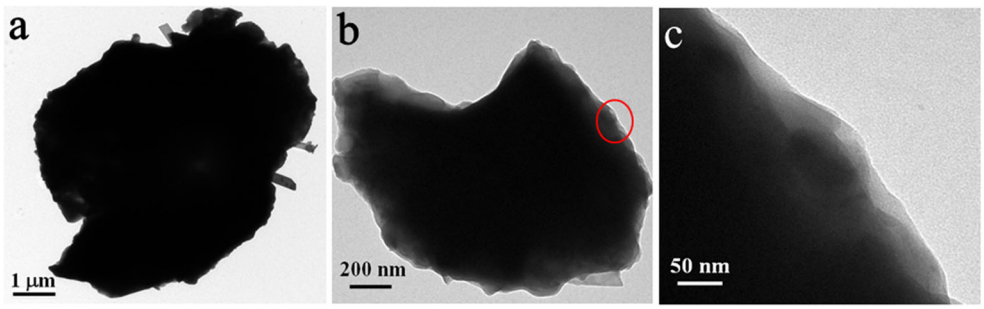

Fig. 5 TEM images of (**a**) unmodified, (**b**) KH-570 modified silicon nitride powders and (**c**) is a partial enlargement of (**b**)

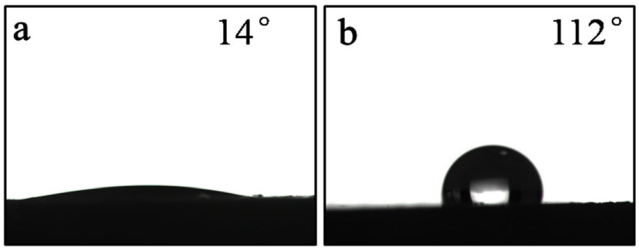

Fig. 6 Water contact angle of silicon nitride modified with KH-570 (a: silicon nitride, b: modified silicon nitride)

EIS measurements

Figure 8 shows the Nyquist diagrams and Bode plots measured on epoxy coating, unmodified silicon nitride coating and modified silicon nitride coating in 3.5 wt% NaCl solution, respectively. The impedance modulus at the low frequency of 0.01 Hz ($|Z|_{0.01Hz}$) can be used to approximately evaluate the corrosion resistance of coatings [12, 56]. Initially, the epoxy coating has a $|Z|_{0.01Hz}$ value of 7.7×10^8 Ω cm^2 (Fig. 8 (a)). After 4 h of immersion, the $|Z|_{0.01Hz}$ is reduced to 1.5×10^8Ω cm^2. After 48 h of immersion, the $|Z|_{0.01Hz}$ is decreased to 2.9×10^6 Ω cm^2. With increasing the immersion time, the low-frequency impedance decreases continuously. This indicates that the epoxy coating is not durable upon long-term immersion in the chloride solution. For unmodifed silicon nitride coating (Fig. 8 (d)), the $|Z|_{0.01Hz}$ is much higher than that measured for the epoxy coating at individual immersion time. It decreases gradually from 8.5×10^{10} Ω cm^2 to 1.7×10^8 Ω cm^2 with the increase of immersion time, and maintains at this value after 432 h. Obviously, the addition of silicon nitride pigment improves the corrosion resistance of the coating, but still suffers from long term degradation.

For modified silicon nitride coating, the initial $|Z|_{0.01Hz}$ value is about 1.2×10^{11} Ω cm^2, which is the highest of all coatings. After 240-h immersion, it is still at 3.7×10^{10} Ω cm^2. The $|Z|_{0.01Hz}$ gradually increases to 7.9×10^{10} Ω cm^2 after 1200-h immersion, and maintains a high corrosion resistance (5.7×10^{10} Ω cm^2) until 2400-h immersion. It is thus seen that the $|Z|_{0.01Hz}$ value of the modified coating is five and three orders of magnitude higher than that of the epoxy coating and the coating doped with unmodified silicon nitride. The modified silicon nitride remarkably enhances the corrosion resistance of the epoxy coating.

To further analyze the impedance data, the electrochemical equivalent circuit in Fig. 9 is used to fit the recorded EIS results, R_s is solution resistance, $C_{coating}$ and $R_{coating}$ are the coating capacitance and coating pore resistance, respectively, Q_{dl} is the constant phase element representing the double layer capacitance, and R_t is the charge transfer resistance. Initially, the Nyquist plots of epoxy coating (Fig. 8 (b)) at 0.5 h of immersion exhibit diffusive impedance, and the equivalent circuit in Fig. 9 (c) is used for fitting. With the increase of the immersion time, the Nyquist plot of epoxy coating (Fig. 8 (c)) exhibits two capacitive loops, and the equivalent circuit in Fig. 9 (b) is used. For the coating doped with unmodified silicon nitride (Fig. 8 (e)), a pure capacitive loop is observed. The circuit in Fig. 9 (a) is used for impedance fitting. With the increase of the immersion time, two capacitive loops are observed, and the equivalent circuit in Fig. 9 (b) is used. For the modified silicon nitride coating, a pure capacitive loop shows and the equivalent circuit in Fig. 9 (a) is used for fitting. As the increase of the immersion time, two time constants appear, and the equivalent circuit in Fig. 9 (b) is used.

The pore resistance ($R_{coating}$) and charge transfer resistance (R_t) can serve as evaluation indexes of coating performance [12, 13, 57, 58]. Generally, with the increase of immersion time, $R_{coating}$ decreases, which is attributed to the penetration of electrolyte through the coating pores. The time dependence of $R_{coating}$ is shown in Fig. 10 (a). It is seen that the resistance of epoxy coating decreases significantly from 2.8×10^8 to 2.7×10^6 Ω cm^2 after 30-h immersion, and then the coating resistance further reduces to 4.9×10^5 Ω cm^2 at 312 h. After that, the coating resistance fluctuates around $10^5 \sim 10^6$ Ω cm^2. For the coating doped with as-received silicon nitride, the coating resistance is 1.2×10^{11} Ω cm^2 at the beginning, which is about three order of magnitude higher than that of the epoxy coating. However, the $R_{coating}$ value dramatically decreases to 2.0×10^8 Ω cm^2 after 84-h immersion. With increasing the time, the $R_{coating}$ continuously decreases to 1.6×10^5 Ω cm^2 at 312 h of immersion, which is similar to that of epoxy coating. After 312 h of immersion, the $R_{coating}$ fluctuates at the range of $4.5\times10^{8-}2.5\times10^7$ Ωcm^2. The coating

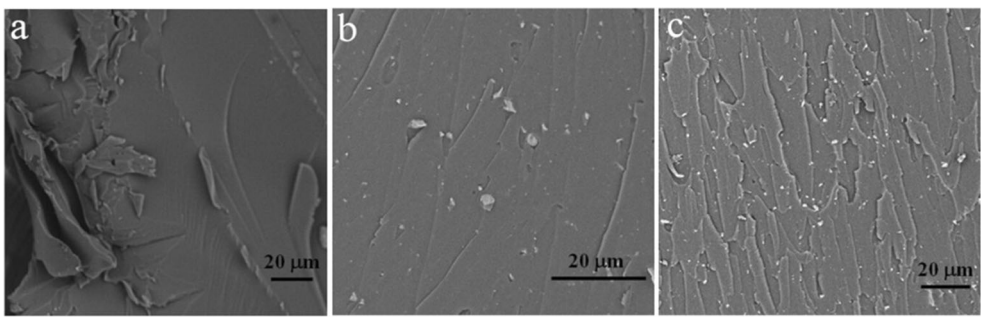

Fig. 7 SEM images of (**a**) epoxy coating, (**b**) unmodified silicon nitride coating and (**c**) modified silicon nitride coating (**a-c** cross-sections)

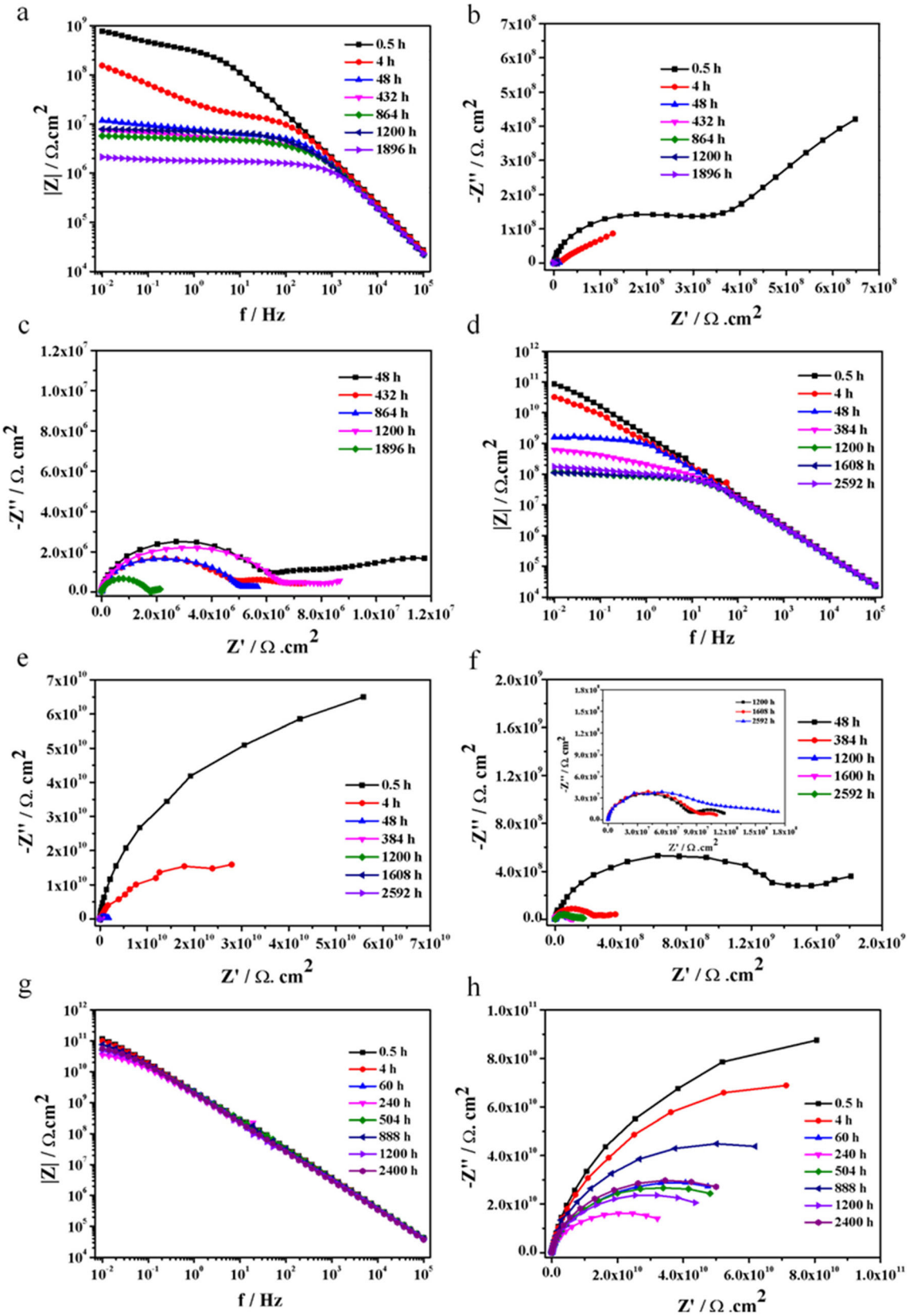

Fig. 8 Impedance plots of different coatings (**a**-**c**) epoxy resin coating, (**d**-**f**) unmodified silicon nitride coating, and (**g**-**h**) modified silicon nitride coating ((**c**) and (**f**) are the enlarged part of (**b**) and (**e**), respectively)

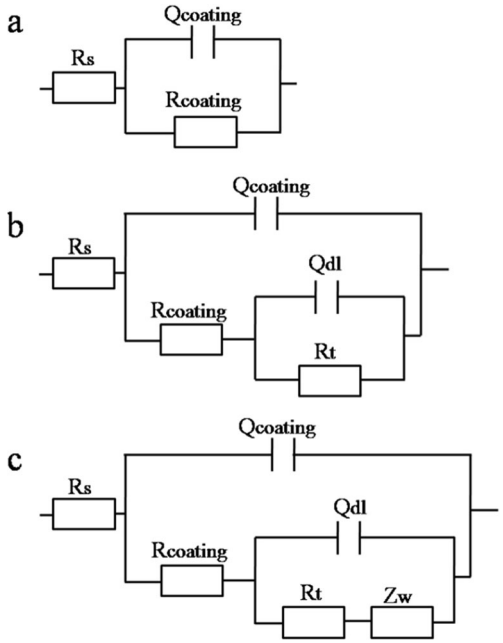

Fig. 9 Equivalent electrical circuits used to fit the measured impedance data for the coatings

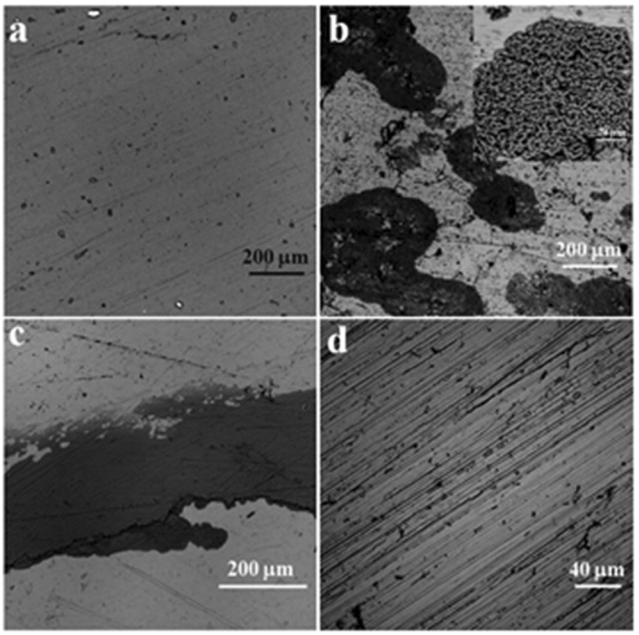

Fig. 11 SEM images of (**a**) original Q235 carbon steel and substrate corrosion morphology beneath coatings after electrochemical impedance measurement (**b**) beneath epoxy resin coating, (**c**) beneath unmodified silicon nitride coating, (**d**) beneath modified silicon nitride coating

resistance value of the modified silicon nitride coating is the highest of all the coatings, which is 1.9×10^{11} Ω cm^2 initially. With the increase of the time, the $R_{coating}$ value reduces slightly, and fluctuates at 3.7×10^{10} Ω cm^2–1.9×10^{9} Ω cm^2 after 1344 h of immersion.

The charge transfer resistance R_t measures the electron transfer across the metal surface, and a higher R_t value indicates a lower corrosion rate. Figure 10(b) shows the R_t values of epoxy coating, the coating doped with as-received silicon nitride, and the modified silicon nitride coating. The R_t value of epoxy coating decreases from 6.7×10^{8} to 7.7×10^{6} Ω cm^2 during 192-h immersion, and remains at the range of 1.0×10^{7}–5×10^{5} Ω cm^2. The R_t value of the unmodified silicon nitride coating reaches 1.3×10^{10} Ω cm^2 in the initial immersion, and gradually decreases to 5×10^{7}Ω cm^2 after 1104-h immersion. However, for the modified silicon nitride coating, the R_t value of 1.1×10^{11} Ω cm^2 is recorded at the beginning of immersion, and has a slight decrease until 2400-h immersion. With increasing the time, the R_t value slightly fluctuates, but still remains at a higher value than epoxy coating and the unmodified silicon nitride coating. This, the results indicate that the modified silicon nitride coating could provide a higher R_t

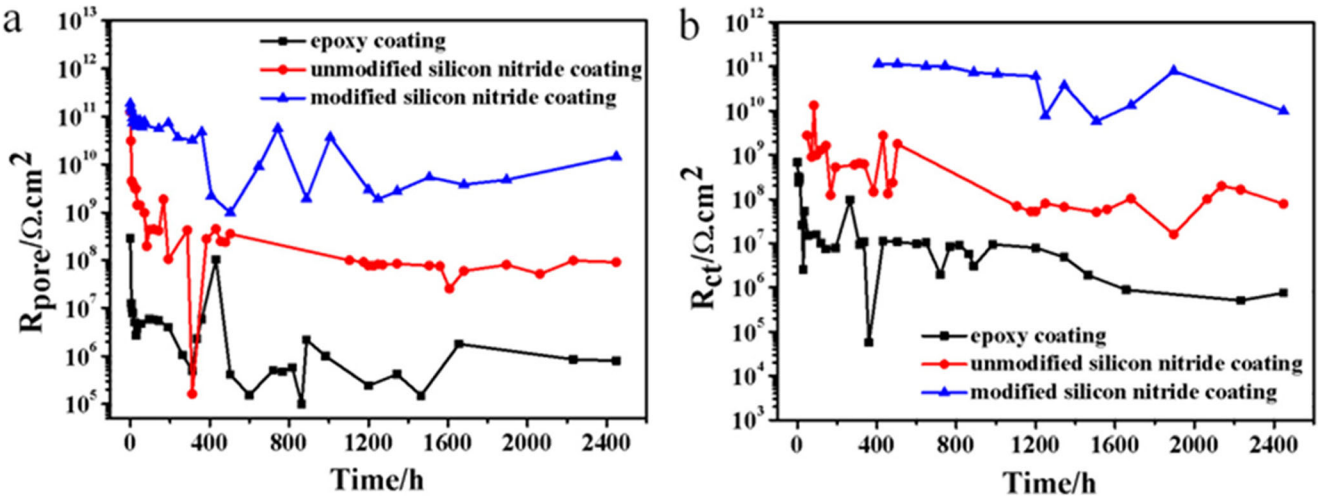

Fig. 10 The coating pore resistance $R_{coating}$ (**a**) and charge transfer resistances R_{ct} (**b**) as a function of the immersion time of the epoxy coating, unmodified silicon nitride coating and modified silicon nitride coating in 3.5% NaCl solution

Table 2 The weight percentage of the elements in substrate for coatings

Coatings substrate	Fe%	O%	C%	Cl%	Na%
original sample	96.26	3.56	0.18		
epoxy resin	61.36	28.46	3.48	3.36	3.34
unmodified	61.97	33.28	3.37	1.38	
modified	85.10	14.65	0.45		

Table 3 Diffusion coefficient of epoxy resin, unmodified and modified silicon nitride coatings

coatings	L (μm)	m_s (mg)	$D \times 10^{-10}$(cm^2 s^{-1})
epoxy resin	308	144.3	10.05
unmodified	255	134.8	5.45
modified	293	137.4	1.10

value and reduces the steel corrosion effectively. The results of electrochemical impedance spectroscopy (EIS) demonstrated that the silicon nitride coating shows better corrosion resistance ability than previous reports using other pigments as shown in Table S1.

Surface analysis

The EDS of original carbon steel Q235 and corrosion morphologies of the carbon steel Q235 after electrochemical impedance measurement (2400 h of immersion) beneath the epoxy resin coating, silicon nitride coating and modified silicon nitride coating are shown in Fig. 11. Many deep corrosion pits and corrosion products can be observed distributing on the surface of the Q235 beneath epoxy resin coating (Fig. 11(b)). Similarly, many corrosion products are also observed beneath unmodified silicon nitirde coating (Fig. 11(c)). However, no visible corrosion products except for original Q235 surface defects on the surface of the Q235 beneath modified silicon nitride coating (Fig. 11(d)). The SEM analysis results also indicate that modified silicon nitride coating can protect carbon steel from corrosion, which is consistent with the EIS analysis. In order to further confirm the results of EIS, EDS analysis were made on the surface of the metal substrate under the coating in Table 2. The results showed that the compositions of the Q235 surface beneath epoxy resin coating included Fe, C, O, Cl and Na; meanwhile the ratio of Fe and O changed largely compared with original Q235 carbon steel, which indicated that corrosive ions diffused inside the coating through pores. Similarly, the Q235 surface of protected by unmodified coating was consisted of Fe, C, O, and Cl; in addition the ratio of Fe and O also changed largely compared with original Q235 carbon steel. However, the Q235 surface of protected by unmodified coating consisted of Fe, C and O; besides the content of elemental composition changed a little compared with original Q235 carbon steel. The presence of Cl element in Q235 protected by epoxy coatings and unmodified coatings demonstrated that the existence of corrosion products, which proved the high corrosion resistance of modified silicon nitride coatings. These results confirm that the modified silicon nitride coating enhanced the corrosion resistance of the coating. Therefore, modified silicon nitirde coating can provide strongest barrier for corrosive ions among three coatings. The EDS elements mapping of different samples was shown in FigS4- S7.

Water absorption

Resistance to water absorption of organic coatings is critical to the performance and corrosion protection in the service

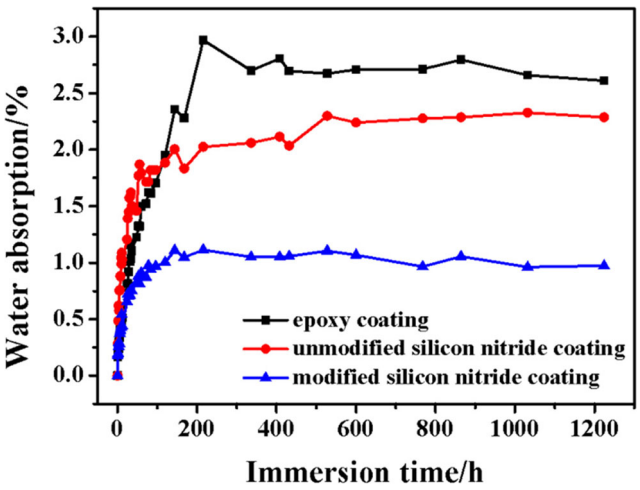

Fig. 12 Water absorption curves of epoxy coating, unmodified silicon nitride coating and the modified silicon nitride coating

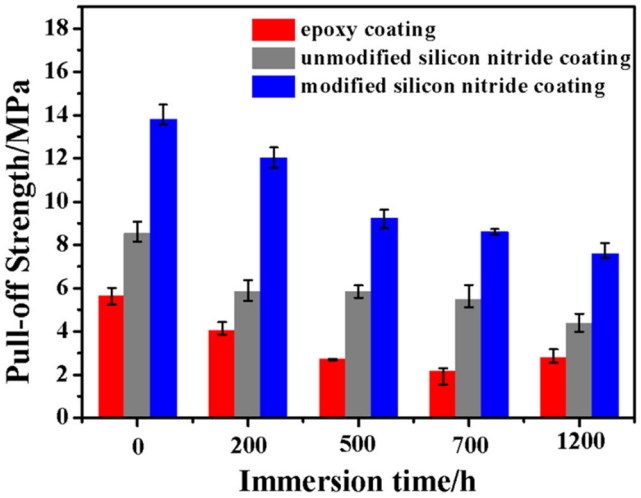

Fig. 13 The adhesion strength of epoxy coating, unmodified silicon nitride coating and modified silicon nitride coating as a function of immersion time

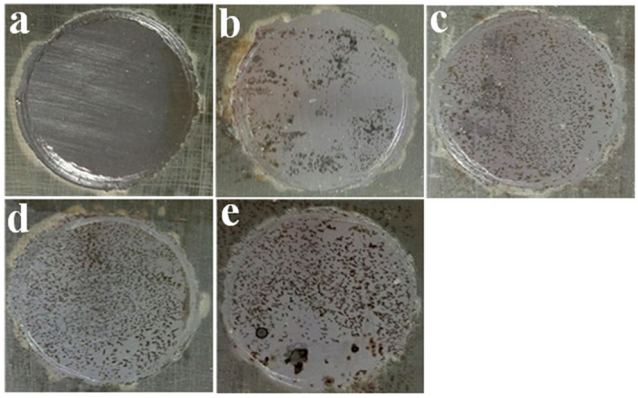

Fig. 14 Epoxy coating failure after pull off test after (**a**) 0 h, (**b**) 200 h, (**c**) 500 h, (**d**) 700 h and (**e**) 1200 h in the chloride solution

[59–61]. Figure 12 shows the water absorption curve of epoxy coating, coating doped with unmodified silicon nitride and the modified silicon nitride coating. It is seen that the water absorption curves of all coatings have a similar tendency. They all include two stages, i.e., the water absorption of the coatings increase quickly initially, and then reaches a saturation stage. For the modified silicon nitride coating, the water absorption increases at the lowest rate, and the water absorption reaches saturation after 408-h immersion in a 3.5% NaCl solution. Moreover, the modified silicon nitride coating absorbs the least water among the three coatings at saturation. The results further confirm that the modified silicon nitride coating could provide an effective barrier to penetrate the electrolyte solution. Generally, water absorption is related to the coating thickness of and the diffusion coefficient of water in the coating as shown by Eq. (1) [62, 63]:

$$\frac{m_t}{m_s} = \frac{4\sqrt{D}}{L\sqrt{\pi}}\sqrt{t} \quad (1)$$

where m_t and m_s are water absorption at time t and the saturation water absorption, respectively, L is the coating

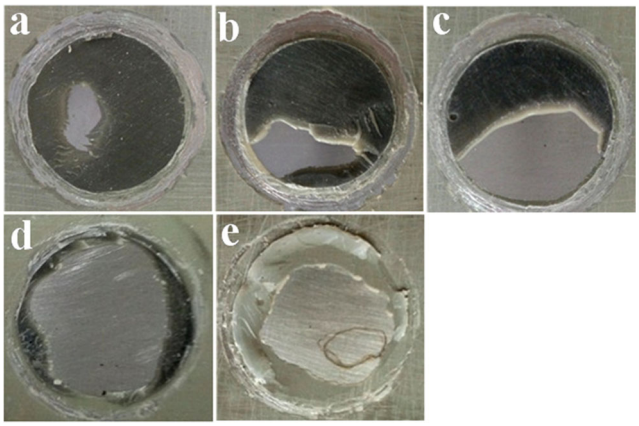

Fig. 15 Unmodified silicon nitride coating failure after pull off test after (**a**) 0 h, (**b**) 200 h, (**c**) 500 h, (**d**) 700 h and (**e**) 1200 h in the chloride solution

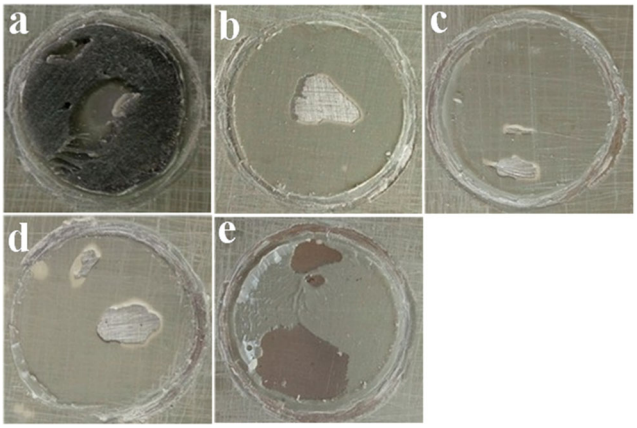

Fig. 16 Modified silicon nitride coating failure after pull off test after (**a**) 0 h, (**b**) 200 h, (**c**) 500 h, (**d**) 700 h and (**e**) 1200 h in the chloride solution

thickness, D is the diffusion coefficient, and t is the immersion time. Table 3 shows the calculated results, which indicate that the modified silicon nitride coating has a low diffusion coefficient of 1.10×10^{-10}(cm^2 s^{-1}).

Pull-off adhesion measurements

A high adhesion strength is essential to the anticorrosive performance of the coatings [19, 64]. Figure 13 shows the results of adhesion strength of various coatings. Before immersion in 3.5 wt% NaCl solution, the adhesion strengths of epoxy coating, unmodified silicon nitride coating and the modified silicon nitride coating are 5.6, 8.6 and 13.8 MPa, respectively, which indicate that the incorporation of modified silicon nitride into the epoxy coating increases the adhesion of the epoxy coating to the steel substrate. The silane-modified silicon nitride coating shows better adhesion strength ability than previous reports using other inorganic pigments as shown in Table S2.

With increasing the immersion time, the adhesion strength of epoxy coating and the unmodified silicon nitride coating sharply decreases. After 1200-h immersion, the adhesion strength of the epoxy coating and the unmodified silicon nitride coating is reduced to 2.8 and 4.4 MPa, respectively. However, the adhesion strength of the modified silicon nitride coating maintains 7.6 MPa. It is thus seen that the modified silicon nitride coating remains the highest adhesion strength among the three coatings after immersion in the chloride solution.

Figure 14 shows the surface morphologies after adhesion measurement of epoxy coating as a function of time in the chloride solution. It is seen that corrosion products appear on the whole surface of the specimen after 200-h immersion in the solution. Corrosion of the steel becomes more serious with increasing the time. Corrosive ions diffuse to the epoxy-resin/carbon steel interface, resulting in delamination of the epoxy coating.

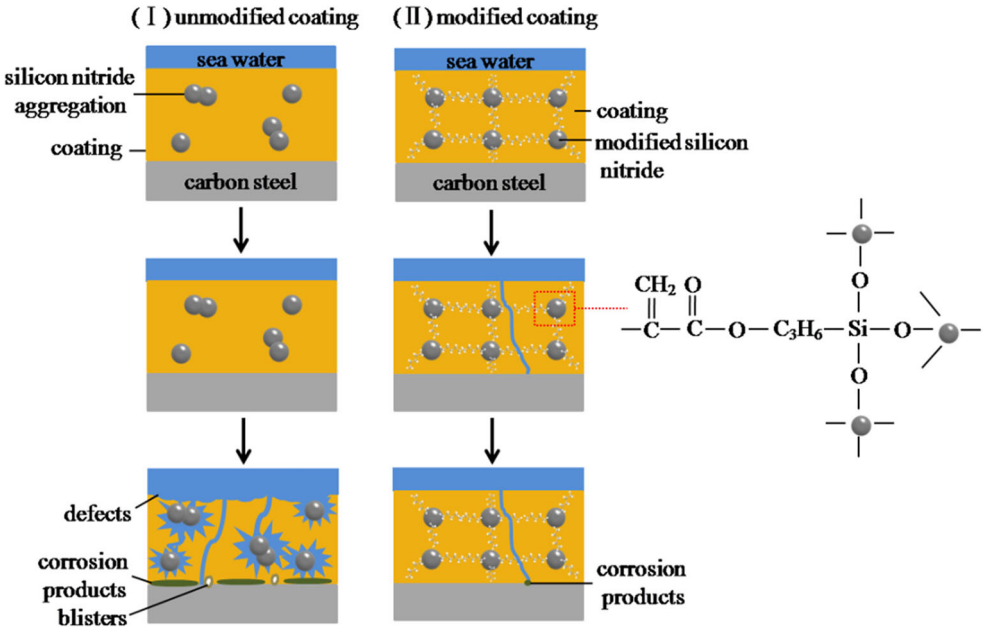

Fig. 17 The possible protection mechanism of different coatings

Figure 15 shows the surface morphologies after adhesion measurement of the unmodified silicon nitride coating with the immersion time. The corrosion products appear after 1200-h immersion. The unmodified silicon nitride coating could provide anticorrosive performance than the epoxy coating. Figure 16 shows the surface morphologies after adhesion measurement of the modified silicon nitride coating with time. The surface of the coating is partially peeled off, without corrosion products beneath the coating. It is thus clear that the modified silicon nitride coating could improve the adhesion strength of the coating and protect the steel from corrosion attack.

Mechanism for corrosion protection of the modified silicon nitride epxoy coatings

This work confirms that the modified silicon nitride epoxy coating significantly increases the anticorrosive performance of the coating. Figure 17 shows the mechanism of the corrosion protection offered by the modified silicon nitride coating and unmodified coating. Epoxy coatings could not stop penetration of water into the coating, resulting in coating degradation. The unmodified silicon nitride coating generates interface gaps around silicon nitride powders due to poor dispersibility, causing the weak boding between the silicon nitride and epoxy. Once water diffuses into the coating, hydrophilic silicon nitride powders (Fig. 6) cause water to collect at the interface between silicon nitride and epoxy. Consequently, protection performance of the coating is lost. However, the modified silicon nitride coating can protect the steel from corrosion due to strong blocking barrier of the hydrophobic surface and the bonding force between the silicon nitride powders and epoxy [65]. Therefore, the diffusion of corrosive ions and water into the modified silicon nitride coating becomes more difficult than the unmodified silicon nitride coating and epoxy coating.

The effective blocking barrier effect offered by the modified silicon nitride coating could impede the penetration of water and corrosive ions to the interface of the coating/steel, and improve the protective properties due to the hydrophobic nature of the modified silicon nitride powders. In addition, the modified silicon nitride powders form a bonding force with the epoxy coating, which also increases the adhesion strength of coating. With the increase of the immersion time, the modified silicon nitride coating can maintain a high adhesion strength and coating resistance, reducing the steel corrosion effectively.

Conclusions

Silicon nitride was firstly used as anti-corrosive pigment in organic coatings. Moreover, an effective strategy by combining inorganic fillers and organosilanes was proposed to enhance the dispersibility of silicon nitride in epoxy resin and applied to protect Q235 carbon steel. The results indicated that modified silicon nitride coating exhibited good anticorrosion performance, which could be attributed to two aspects. On one hand, KH-570 was employed to increase the possible chemical interactions between silicon nitride powders and epoxy resin. In addition, the dispersibility of silicon nitride was enhanced significantly due to the modification with KH-570. On the other hand, modified silicon nitride coating significantly influenced the barrier performance due to hydrophobic

surface of modified silicon nitride powder and made the corrosive electrolyte diffusion pathways more tortuous. Consequently, the strategy proposed in this paper can be a guide for design anticorrosive coatings. The modified silicon nitride coating shows better corrosion resistance ability than previous reports used other pigments (Table S1).

Acknowledgements This work was supported by the National Natural Science Foundation (51572249), the Natural Science Foundation for Shandong Province (ZR2014EMM021), the National High Technology Research and Development Programof China (2013A2041106), and the Fundamental Research Funds for the Central Universities (841562011).

References

1. Kumar SA, Denchev Z (2009) Development and characterization of phosphorus-containing siliconized epoxy resin coatings. Prog Org Coat 66:1–7
2. Kang Y, Chen X, Song S, Yu L, Zhang P (2012) Friction and wear behavior of nanosilica-filled epoxy resin composite coatings. Appl Surf Sci 258:6384–6390
3. Asiri AM, Hussein MA, Abu-Zied BM, Hermas A-EA (2013) Effect of NiLaxFe2−xO4 nanoparticles on the thermal and coating properties of epoxy resin composites. Compos Part B 51:11–18
4. Brostow W, Dutta M, Rusek P (2010) Modified epoxy coatings on mild steel: tribology and surface energy. Eur Polym J 46:2181–2189
5. Legghe E, Aragon E, Bélec L, Margaillan A, Melot D (2009) Correlation between water diffusion and adhesion loss: study of an epoxy primer on steel. Prog Org Coat 66:276–280
6. Popineau S, Rondeau-Mouro C, Sulpice-Gaillet C, Shanahan MER (2005) Free/bound water absorption in an epoxy adhesive. Polymer 46:10733–10740
7. Sørensen PA, Kiil S, Dam-Johansen K, Weinell CE (2009) Anticorrosive coatings: a review. J Coat Technol Res 6:135–176
8. Le Pen C, Lacabanne C, Pébère N (2000) Structure of waterborne coatings by electrochemical impedance spectroscopy and a thermostimulated current method: influence of fillers. Prog Org Coat 39:167–175
9. Veleva L, Chin J, del Amo B (1999) Corrosion electrochemical behavior of epoxy anticorrosive paints based on zinc molybdenum phosphate and zinc oxide. Prog Org Coat 36:211–216
10. Vilche JR, Bucharsky EC, Giúdice CA (2002) Application of EIS and SEM to evaluate the influence of pigment shape and content in ZRP formulations on the corrosion prevention of naval steel. Corros Sci 44:1287–1309
11. Bierwagen G, Battocchi D, Simões A, Stamness A, Tallman D (2007) The use of multiple electrochemical techniques to characterize mg-rich primers for Al alloys. Prog Org Coat 59:172–178
12. Liu X, Shao Y, Zhang Y, Meng G, Zhang T, Wang F (2015) Using high-temperature mechanochemistry treatment to modify iron oxide and improve the corrosion performance of epoxy coating – I. High-temperature ball milling treatment. Corros Sci 90:451–462
13. Liu X, Shao Y, Zhang Y, Meng G, Zhang T, Wang F (2015) Using high-temperature mechanochemistry treatment to modify iron oxide and improve the corrosion performance of epoxy coating – II. Effect of grinding temperature. Corros Sci 90:463–471
14. Chen S, Cai Y, Zhuang C, Yu M, Song X, Zhang Y (2015) Electrochemical behavior and corrosion protection performance of bis[triethoxysilylpropyl] tetrasulfide silane films modified with TiO_2 sol on 304 stainless steel. Appl Surf Sci 331:315–326
15. Balaskas AC, Kartsonakis IA, Tziveleka LA, Kordas GC (2012) Improvement of anti-corrosive properties of epoxy-coated AA 2024-T3 with TiO2 nanocontainers loaded with 8-hydroxyquinoline. Prog Org Coat 74:418–426
16. Al-Turaif HA (2010) Effect of nano TiO2 particle size on mechanical properties of cured epoxy resin. Prog Org Coat 69:241–246
17. Gupta G, Birbilis N, Cook AB, Khanna AS (2013) Polyaniline-lignosulfonate/epoxy coating for corrosion protection of AA2024-T3. Corros Sci 67:256–267
18. Pereira da Silva JE, Córdoba de Torresi SI, Torresi RM (2005) Polyaniline acrylic coatings for corrosion inhibition: the role played by counter-ions. Corros Sci 47:811–822
19. Zhang Y, Shao Y, Zhang T, Meng G, Wang F (2011) The effect of epoxy coating containing emeraldine base and hydrofluoric acid doped polyaniline on the corrosion protection of AZ91D magnesium alloy. Corros Sci 53:3747–3755
20. Vakili H, Ramezanzadeh B, Amini R (2015) The corrosion performance and adhesion properties of the epoxy coating applied on the steel substrates treated by cerium-based conversion coatings. Corros Sci 94:466–475
21. Yang C, Wei H, Guan L, Guo J, Wang Y, Yan X, Zhang X, Wei S, Guo Z (2015) Polymer nanocomposites for energy storage, energy saving, and anticorrosion. J Mater Chem A 3:14929–14941
22. Ji W-G, Hu J-M, Zhang J-Q, Cao C-N (2006) Reducing the water absorption in epoxy coatings by silane monomer incorporation. Corros Sci 48:3731–3739
23. Wu L-K, Zhang J-T, Hu J-M, Zhang J-Q (2012) Improved corrosion performance of electrophoretic coatings by silane addition. Corros Sci 56:58–66
24. Ji W-G, Hu J-M, Liu L, Zhang J-Q, Cao C-N (2006) Water uptake of epoxy coatings modified with γ-APS silane monomer. Prog Org Coat 57:439–443
25. Jiang M-Y, Wu L-K, Hu J-M, Zhang J-Q (2015) Silane-incorporated epoxy coatings on aluminum alloy (AA2024). Part 1: improved corrosion performance. Corros Sci 92:118–126
26. Jiang M-Y, Wu L-K, Hu J-M, Zhang J-Q (2015) Silane-incorporated epoxy coatings on aluminum alloy (AA2024). Part 2: mechanistic investigations. Corros Sci 92:127–135
27. Lee MR, Russell SS, Arden JW, Pillinger CT (1995) Nierite (Si3N4), a new mineral from ordinary and enstatite chondrites. Meteoritics 30:387–398
28. Lukianova O (2015) Mechanical and elastic properties of new silicon nitride ceramics produced by cold isostatic pressing and free sintering. Ceram Int 41 (13716–13720
29. Seiner H, Ramirez C, Koller M, Sedlák P, Landa M, Miranzo P, Belmonte M, Osendi MI (2015) Elastic properties of silicon nitride ceramics reinforced with graphene nanofillers. Mater Des 87:675–680
30. Riley FL (2004) Silicon nitride and related materials. J Am Ceram Soc 83:245–265
31. Yu J, Wang H, Zhang J (2009) Neural network modeling and analysis of gel casting preparation of porous Si3N4 ceramics. Ceram Int 35:2943–2950
32. Lyckfeldt O, Ferreira JMF (1998) Processing of porous ceramics by 'starch consolidation'. J Eur Ceram Soc 18:131–140
33. Blugan G, Wittig D, Kuebler J (2009) Oxidation and corrosion of silicon nitride ceramics with different sintering additives at 1200 and 1500°C in air, water vapour, SO2 and HCl environments – a comparative study. Corros Sci 51:547–555
34. Klemm H (2010) Silicon nitride for high-temperature applications. J Am Ceram Soc 93:1501–1522
35. Jordache MK, Du H (2015) High-temperature alkali corrosion of Kyocera SN282 silicon nitride. Corros Sci 91:68–74
36. Monteverde F, Mingazzini C, Giorgi M, Bellosi A (2001) Corrosion of silicon nitride in sulphuric acid aqueous solution. Corros Sci 43:1851–1863

37. Dierksen D, Kühner P, Kappler A, Nickel KG (2011) Microbial corrosion of silicon nitride ceramics by sulphuric acid producing bacteria Acidithiobacillus ferrooxidans. J Eur Ceram Soc 31:1177–1185
38. Olofsson J, Pettersson M, Teuscher N, Heilmann A, Larsson K, Grandfield K, Persson C, Jacobson S, Engqvist H (2012) Fabrication and evaluation of SixNy coatings for total joint replacements. J Mater Sci Mater Med 23:1879–1889
39. Pettersson M, Berlind T, Schmidt S, Jacobson S, Hultman L, Persson C, Engqvist H (2013) Structure and composition of silicon nitride and silicon carbon nitride coatings for joint replacements. Surf Coat Technol 235:827–834
40. Pettersson M, Tkachenko S, Schmidt S, Berlind T, Jacobson S, Hultman L, Engqvist H, Persson C (2013) Mechanical and tribological behavior of silicon nitride and silicon carbon nitride coatings for total joint replacements. J Mech Behav Biomed Mater 25:41–47
41. Li Y, Qu L, Wang F (2003) The electrochemical corrosion behavior of TiN and (Ti,Al)N coatings in acid and salt solution. Corros Sci 45:1367–1381
42. Liu Y, Wang J, Liu L, Li Y, Wang F (2013) Study of the failure mechanism of an epoxy coating system under high hydrostatic pressure. Corros Sci 74:59–70
43. Tian W, Liu L, Meng F, Liu Y, Li Y, Wang F (2014) The failure behaviour of an epoxy glass flake coating/steel system under marine alternating hydrostatic pressure. Corros Sci 86:81–92
44. Ramezanzadeh B, Ahmadi A, Mahdavian M (2016) Enhancement of the corrosion protection performance and cathodic delamination resistance of epoxy coating through treatment of steel substrate by a novel nanometric sol-gel based silane composite film filled with functionalized graphene oxide nanosheets. Corros Sci 109:182–205
45. Lu X, Zuo Y, Zhao X, Tang Y (2012) The improved performance of a mg-rich epoxy coating on AZ91D magnesium alloy by silane pretreatment. Corros Sci 60:165–172
46. Bahlakeh G, Ramezanzadeh B, Ramezanzadeh M (2017) Cerium oxide nanoparticles influences on the binding and corrosion protection characteristics of a melamine-cured polyester resin on mild steel: an experimental, density functional theory and molecular dynamics simulation study. Corros Sci 118:69–83
47. Ku S-L, Lee C-C (2010) Optical and structural properties of silicon nitride thin films prepared by ion-assisted deposition. Opt Mater 32:956–960
48. Brunet M, Aureau D, Chantraine P, Guillemot F, Etcheberry A, Gouget-Laemmel AC, Ozanam F (2017) Etching and chemical control of the silicon nitride surface. ACS Appl Mater Interfaces 9:3075–3084
49. Wang C, Mao H, Wang C, Fu S (2011) Dispersibility and hydrophobicity analysis of titanium dioxide nanoparticles grafted with Silane coupling agent. Ind Eng Chem Res 50:11930–11934
50. Ni W, Wu S, Ren Q (2012) Preparation and characterization of Silanized TiO2Nanoparticles and their application in toner. Ind Eng Chem Res 51:13157–13163
51. Tai Y, Qian J, Zhang Y, Huang J (2008) Study of surface modification of nano-SiO2 with macromolecular coupling agent (LMPB-g-MAH). Chem Eng J 141:354–361
52. Xiao X, Xu R (2011) Preparation and surface properties of core-shell polyacrylate latex containing fluorine and silicon in the shell. J Appl Polym Sci 119:1576–1585
53. Chen L, Jin H, Xu Z, Shan M, Tian X, Yang C, Wang Z, Cheng B (2014) A design of gradient interphase reinforced by silanized graphene oxide and its effect on carbon fiber/epoxy interface. Mater Chem Phys 145:186–196
54. Pan M, Gan X, Mei C, Liang Y (2017) Structural analysis and transformation of biosilica during lignocellulose fractionation of rice straw. J Mol Struct 1127:575–582
55. Hu X, Su E, Zhu B, Jia J, Yao P, Bai Y (2014) Preparation of silanized graphene/poly(methyl methacrylate) nanocomposites in situ copolymerization and its mechanical properties. Compos Sci Technol 97:6–11
56. Chen Y, Wang XH, Li J, Lu JL, Wang FS (2007) Long-term anti-corrosion behaviour of polyaniline on mild steel. Corros Sci 49:3052–3063
57. Shao Y, Huang H, Zhang T, Meng G, Wang F (2009) Corrosion protection of mg–5Li alloy with epoxy coatings containing polyaniline. Corros Sci 51:2906–2915
58. Hao Y, Liu F, Han E-H, Anjum S, Xu G (2013) The mechanism of inhibition by zinc phosphate in an epoxy coating. Corros Sci 69:77–86
59. Pourhashem S, Vaezi MR, Rashidi A, Bagherzadeh MR (2017) Exploring corrosion protection properties of solvent based epoxy-graphene oxide nanocomposite coatings on mild steel. Corros Sci 115:78–92
60. Zhang SY, Li SJ, Luo XW, Zhou WF (2000) Mechanism of the significant improvement in corrosion protection by lowering water sorption of the coating. Corros Sci 42:2037–2041
61. Zhang SY, Ding YF, Li SJ, Luo XW, Zhou WF (2002) Effect of polymeric structure on the corrosion protection of epoxy coatings. Corros Sci 44:861–869
62. Chen Y, Lin A, Gan F (2006) Improvement of polyacrylate coating by filling modified nano-TiO2. Appl Surf Sci 252:8635–8640
63. Becker O, Varley RJ, Simon GP (2004) Thermal stability and water uptake of high performance epoxy layered silicate nanocomposites. Eur Polym J 40:187–195
64. Araujo WS, Margarit ICP, Ferreira M, Mattos OR, Neto PL (2001) Undoped polyaniline anticorrosive properties. Electrochim Acta 46:1307–1312
65. Ramezanzadeh B, Niroumandrad S, Ahmadi A, Mahdavian M, Moghadam MHM (2016) Enhancement of barrier and corrosion protection performance of an epoxy coating through wet transfer of amino functionalized graphene oxide. Corros Sci 103:283–304